Journal of Materials Chemistry C

RSC Publishing

PAPER

View Article Online
View Journal | View Issue

Role of oxadiazole moiety in different D–A polyazothines and related resistive switching properties†

Cite this: *J. Mater. Chem. C*, 2013, **1**, 4556

Liang Pan,‡[abc] Benlin Hu,‡[ab] Xiaojian Zhu,[ab] Xinxin Chen,[ab] Jie Shang,[ab] Hongwei Tan,[ab] Wuhong Xue,[ab] Yuejin Zhu,[c] Gang Liu*[ab] and Run-Wei Li*[ab]

Two donor–acceptor (D–A) polyazothines (PAs), incorporating the oxadiazole entity either acting as an electron acceptor (A) to form D–A structured **PA-1** with the triphenylamine donor (D), or acting as a donor to form D–A structured **PA-2** with the 3,3′-dinitro-diphenylsulfone acceptor, have been successfully synthesized *via* a polycondensation reaction. The variation in the role of the oxadiazole moiety in the D–A polymers, together with the use of different top electrode metals, leads to interesting electronic transport properties and various resistive switching behaviors of the present polyazothines. Pt-electrode devices based on a **PA-1** active layer show a rewritable memory effect with poor endurance (less than 20 cycles), whereas the **PA-2** based Pt devices exhibit write-once read-many-times (WORM) memory behavior. For the Al-electrode devices, both PAs demonstrate a much improved resistive switching effect, and the endurance of the **PA-2** devices is better than that of the **PA-1** devices. The difference in the electronic transport and memory properties of the four devices may originate from the different charge injection/extraction and electron transfer processes of the sandwich systems, and will provide guidelines for selecting both the proper D and A moieties in D–A polymers and electrode metals for high-performance resistance random access memories (RRAMs).

Received 2nd May 2013
Accepted 27th May 2013

DOI: 10.1039/c3tc30826j

www.rsc.org/MaterialsC

Introduction

The resistive switching effect, which refers to the electrical phenomenon that the resistance of a metal/insulator/metal sandwich structure can be reversibly regulated by an external DC or pulse voltage stress,[1–6] has demonstrated potential applications in resistance random access memories (RRAM)[7–20] and artificial neural synapses[21–23] to mimic the functionalities of data storage and logic calculus devices.[24–28] In comparison to their inorganic counterparts, polymeric materials are equally attractive for resistive switching applications due to their alternative advantages of rich chemical diversity, easy solution processability, high mechanical flexibility, low fabrication cost, and three-dimensional stacking capability.[29]

Since 1992, when the donor–acceptor (D–A) approach was introduced for the first time to the design of conjugated polymers,[30] D–A polymers have attracted much attention for promising electronic applications in light-emitting diodes, field effect transistors, solar cells and memory devices.[5,31,32] In particular, electronic memories based on D–A polymers with a large on/off ratio, good endurance, long retention time, low power consumption and fast switching speed have been investigated extensively over the past few years.[33–36] Nevertheless, there are still challenges in D–A polymer memories, where the lack of a comprehensive and clear understanding of the electronic origin that causes the resistance transition hinders the development of high-performance materials for practical memory applications.[37–39]

Poly(Schiff base) materials are a family of conjugated polymers containing imine groups (C=N) in the backbone and exhibiting excellent thermal stability, good mechanical properties, metal-chelating ability and molecular doping-controlled electrical properties.[20,40–42] On the other hand, oxadiazole-based polymers are well known as electron-transporting materials in photoelectric devices, due to their high electron affinity, as well as thermal, hydrolytic, and optical stability.[43,44] Recently, polymers containing either Schiff base or oxadiazole segments have been explored for memory applications, and it is reported that the oxadiazole moieties may turn from an electron acceptor into

[a]*Key Laboratory of Magnetic Materials and Devices, Ningbo Institute of Material Technology and Engineering, Chinese Academy of Sciences, Ningbo 315201, China. E-mail: liug@nimte.ac.cn; runweili@nimte.ac.cn; Fax: +86-574-8668-5163; Tel: +86-574-86685030*

[b]*Zhejiang Province Key Laboratory of Magnetic Materials and Application Technology, Ningbo Institute of Material Technology and Engineering, Chinese Academy of Sciences, Ningbo 315201, China*

[c]*Department of Physics, Ningbo University, Ningbo 315211, China*

† Electronic supplementary information (ESI) available: See DOI: 10.1039/c3tc30826j

‡ Liang Pan and Benlin Hu contributed equally to this work.

an electron donor when bonded to a functional group with stronger electron withdrawing ability.[7,45–48]

In this work, polyazothines based on triphenylamine-oxadiazole (TPA-OXD) and oxadiazole-3,3′-dinitro-diphenylsulfone (OXD-NPS) D–A structures have been synthesized *via* polycondensation reactions. With the different roles of the oxadiazole moiety in the D–A polymers, **PA-1** and **PA-2** exhibit rewritable and write-once read-many-times (WORM) resistive switching behaviors in the Pt/PA/Pt sandwich structures, respectively. When Al is used as the top electrode instead, both polymers exhibit rewritable switching behaviors due to the enhanced carrier extraction under reversed electric fields. These results could provide new insight into the design strategy of high-performance D–A polymers and their resistance random access memory (RRAM) devices.

Experimental section

Materials and synthesis

Hydrazine sulfate, *p*-aminothiophenol, *p*-fluorobenzoic acid, triphenylamine, 4,4′-dichlorodiphenyl sulfone and *p*-hydroxybenzaldehyde were purchased from Aladdin Reagent Co. and used as received. 2,5-bis(4-fluorophenyl)-1,3,4-oxadiazole, 1,3-bis(4-chloro-3-nitrophenyl)sulfone[49] and 4,4′-diformyl-triphenylamine[50] were synthesized and purified according to the literature. All the other reagents and solvents were of analytical grade and used without further purification.

Synthesis of 2,5-bis(*p*-aminophenylthiophenyl)-1,3,4-oxadiazole (M1 in Scheme 1). A mixture of 2,5-bis(4-fluorophenyl)-1,3,4-oxadiazole (5.16 g, 0.020 mol), *p*-aminothiophenol (5.10 g, 0.041 mol), potassium carbonate (5.67 g, 0.041 mol) and *N*,*N*-dimethylformamide (DMF, 40 mL) was placed in a two-necked round-bottom flask and heated to 100 °C for 7 h under vigorous stirring in an argon atmosphere. The mixture was then cooled to room temperature and poured slowly into a water–ethanol mixture (10 : 1, v/v). The white precipitate was filtered, washed with deionized water and dried under reduced pressure at 120 °C overnight. The crude product was recrystallized from tetrahydrofuran–ethanol (13 : 10, v/v), and a colorless needle crystal with a yield of 76.8% (7.20 g) was obtained. FT-IR (cm^{-1}, KBr): 2754 (aldehyde C–H stretching), 3450 and 3371 (NH_2 stretching), 1613 (C=N stretching). Elemental microanalysis, anal. calcd for $C_{26}H_{20}N_4OS_2$: C, 66.64; H, 4.30; N, 11.96; S, 13.69. Found: C, 66.49; H, 4.36; N, 11.98; S, 13.65%. ^{1}H NMR (400 MHz, DMSO-d_6, δ, ppm): 7.93 (4H, d, $J = 8.0$ Hz), 7.23 (4H, d, $J = 8.0$ Hz), 7.16 (4H, d, $J = 8.0$ Hz), 6.66 (4H, d, $J = 8.0$ Hz) and 5.65 (4H, s).

Synthesis of bis-(3-nitro-4-*p*-formylphenyloxy-phenyl) sulfone. A mixture of bis(4-chloro-3-nitrophenyl)sulfone (7.54 g, 0.020 mol), *p*-hydroxybenzaldehyde (4.98 g, 0.041 mol), potassium carbonate (5.80 g, 0.042 mol) and *N*,*N*-dimethylacetamide (DMAc, 100 mL) was placed in a three-necked round-bottom flask and heated to 100 °C for 7 h under vigorous stirring in an argon atmosphere. The mixture was then cooled to room temperature and poured slowly into water (300 mL). The orange precipitate was filtered, washed with deionized water and dried under reduced pressure at 80 °C overnight. The crude product was recrystallized from tetrahydrofuran–water (2 : 1, v/v), and a colorless needle crystal with a yield of 81.2% (8.91 g) was obtained. FT-IR (cm^{-1}, KBr): 2762 (aldehyde C–H stretching), 1698 (aldehyde C=O stretching), 1562 and 1321 ($-NO_2$ stretching), 1338 and 1150 ($-SO_2-$ stretching). Elemental microanalysis, anal. calcd for $C_{26}H_{16}N_2O_8S_3$: C, 53.78; H, 2.78; N, 4.82; S, 16.57. Found: C, 53.52; H, 2.83; N, 4.62; S, 16.38%. ^{1}H NMR (400 MHz, DMSO-d_6, δ, ppm): 9.98 (2H, s), 8.77 (2H, d, $J = 2.4$ Hz), 8.31 (2H, dd, $J = 8.8$ Hz, 2.4 Hz), 7.99 (2H, d, $J = 8.8$ Hz), 7.43–7.36 (6H, m).

Synthesis of PA-1. 4,4′-diformyl-triphenylamine (0.30 g, 1.0 mmol) and **M1** (0.47 g, 1.0 mmol) were dissolved in dry *N*-methyl-2-pyrrolidone (NMP) (6 mL) with *p*-toluenesulfonic acid (0.040 g) as the catalyst. After stirring at 120 °C for 20 h, the mixture was cooled to room temperature and poured slowly into ethanol (100 mL). The precipitate was collected by filtration, washed with hot methanol (on a Soxhlet apparatus) for 24 h, and dried at 80 °C overnight under reduced pressure to give 0.52 g (70.8% yield) of the yellowish **PA-1** powder. FT-IR (cm^{-1}, KBr) (Fig S1†): 1621 (C=N stretching in oxadiazole unit), 1599 (C=N stretching in imine unit). Elemental microanalysis, anal. calcd for $C_{46}H_{31}N_5OS_2$ (repeating unit): C, 75.28; H, 4.26; N, 9.54; S, 8.74. Found: C, 75.31; H, 4.24; N, 9.58; S, 8.71%. ^{1}H NMR (400 MHz, DMF-d_7, δ, ppm): 10.14 (2H, s), 8.08–6.97 (29H, m).

Synthesis of PA-2. This poly(Schiff base) was prepared by a similar procedure to the synthesis of **PA-1**. 0.85 g (86.6% yield) of pale **PA-2** powder was obtained. FT-IR (cm^{-1}, KBr) (Fig. S1†): 1627 (C=N stretching in oxadiazole unit), 1595 (C=N stretching in imine unit), 1498 and 1384 ($-NO_2$ stretching in NPS unit), 1321 and 1158 ($-SO_2-$ stretching in NPS unit). Elemental microanalysis, anal. calcd for $C_{45}H_{31}N_5O_6S_3$ (repeating unit): C, 64.81; H, 3.75; N, 8.40; S, 11.53. Found: C, 64.91; H, 3.71; N, 8.51; S, 11.52%. ^{1}H NMR (400 MHz, DMF-d_7, δ, ppm): 10.10 (2H, s), 8.93–7.32 (30H, m).

Since neither polymer is soluble in tetrahydrofuran (THF) for the determination of molecular weight by standard gel permeation chromatography (GPC) analysis, the inherent viscosity of the PA–NMP solutions were used to evaluate the formation of macromolecules. The as-synthesized **PA-1** and **PA-2** show inherent viscosities of 0.45 dL g^{-1} and 0.51 dL g^{-1} in NMP, respectively, which allow the fabrication of thin polymer films by spin-coating processes.

Memory device fabrication

The Pt/Ti/SiO_2/Si substrates were pre-cleaned in an ultrasonic bath with ethanol, acetone and isopropanol for 20 min each in that order. A 0.1 mL cyclohexanone solution of the PAs was spin-coated onto the substrates at a spinning speed of 400 rpm for 12 s and then 2000 rpm for 40 s, followed by a vacuum-drying treatment at 80 °C for 8 h. Before spin-coating, the solution was filtered through polytetrafluoroethylene (PTFE) membrane micro-filters with a pore size of 0.45 μm to remove undissolved particles. The thickness of the polymer films was about 90 nm, as measured with a spectroscopic ellipsometer (model M2000DI, Woollam). To construct the metal/polymer/Pt sandwich structures, metal top electrodes (Pt or Al) with a diameter

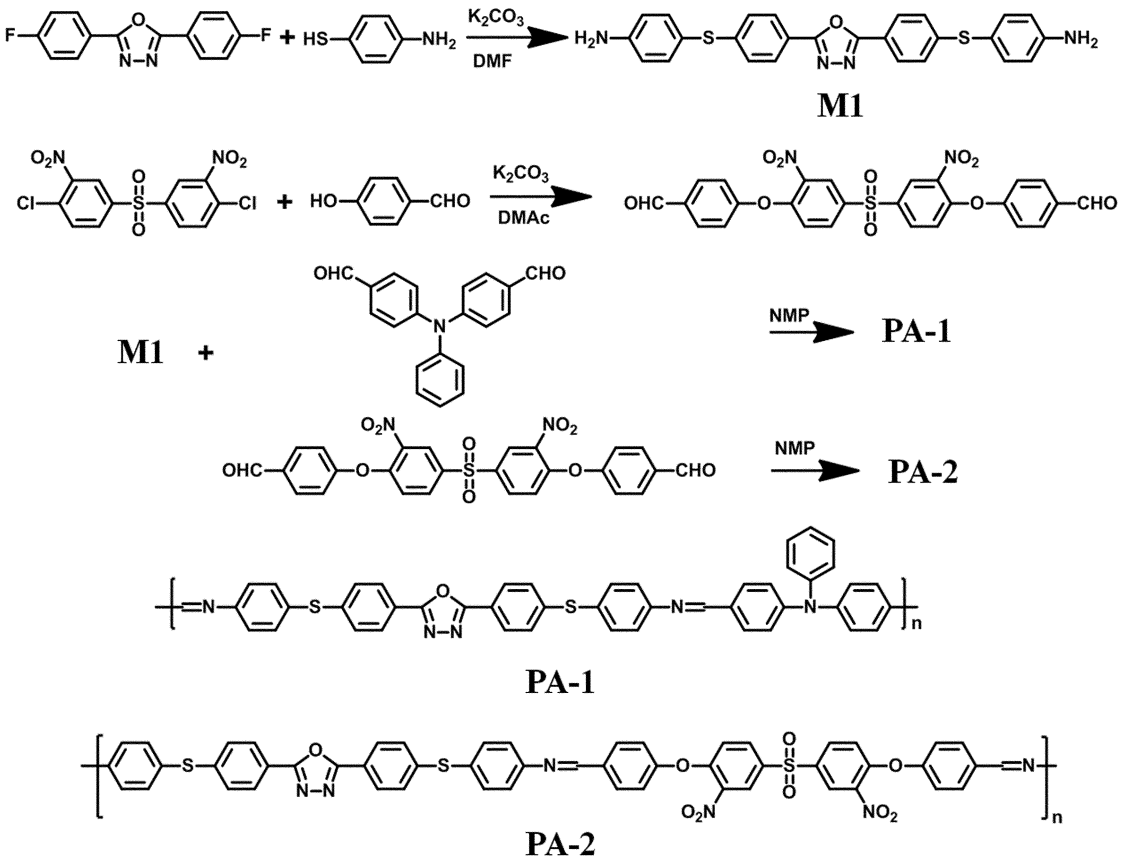

Scheme 1 Synthesis routes for the monomers and poly(Schiff base)s.

of 100 μm and thickness of 150 nm were deposited at room temperature by E-beam evaporation through a metal shadow mask.

Measurements

The current–voltage (*I–V*) characteristics of the metal/polymer/Pt devices were measured in an ambient atmosphere using a Keithley 4200 semiconductor characterization system in the voltage sweeping mode. The sweeping step was 0.01 V. During the measurement, a bias voltage was applied to the top electrodes while the Pt coated substrates were always grounded. Elemental microanalysis (for C, H and N) was performed on an Elementar Vario EL III analyzer. ^{1}H nuclear magnetic resonance (^{1}H NMR) spectra were measured at 400 MHz on a Bruker 400 AVANCE III spectrometer, using dimethyl sulfoxide-d_6 (DMSO-d_6) or *N*,*N*-dimethylformamide-d_7 (DMF-d_7) as the solvent. Fourier transform infrared (FT-IR) spectra were recorded on a Thermo Nicolet 6700 FT-IR spectrometer by dispersing the samples in KBr pellets. The UV-visible absorption spectra were recorded on a Perkin-Elmer lambda 950 spectrophotometer at room temperature.

The inherent viscosities were measured with an Ubbelohde viscometer at 30 ± 0.1 °C in NMP at a concentration of 0.5 g dL^{-1}. Thermogravimetric analysis (TGA) was performed on a Perkin-Elmer Diamond TG/DTA instrument at a heating rate of 10 °C min^{-1} under a nitrogen flow of 50 mL min^{-1}. Differential scanning calorimetry (DSC) measurements were carried out with a Mettler Toledo DSC system at a heating rate of 10 °C min^{-1} under a nitrogen flow of 50 mL min^{-1}, where the glass transition temperature was recorded as the temperature at the middle of the thermal transition from the second heating scan. Gel permeation chromatography traces of the samples were recorded on a Viscotek T60A/LR40 GPC system, where chloroform was used as the eluent, and linear polystyrene was used as the standard. Cyclic voltammetry (CV) measurements were performed on a CHI 650D electrochemical workstation (Chenhua, Shanghai, China) using a three-electrode cell under argon atmosphere. The polymer film coated on a Pt/Ti/SiO_2/Si substrate was scanned in an electrolyte solution of tetrabutylammonium hexafluorophosphate (n-Bu_4NPF_6) in acetonitrile (0.1 M), with a platinum gauze and Ag/AgCl (3.8 M KCl) as the counter and reference electrode, respectively. A scan rate of 100 mV s^{-1} was used during the CV measurements.

Molecular simulation

Calculations of the optimized geometry and electronic structures, including the dipole moment, HOMO, LUMO and electrostatic potential (ESP) surfaces of the donor–acceptor moieties and the basic unit of the PA copolymers were carried out using the Gaussian 09 program package and density functional theory (DFT) methods at the B3LYP/6-31 G(d) level.[51]

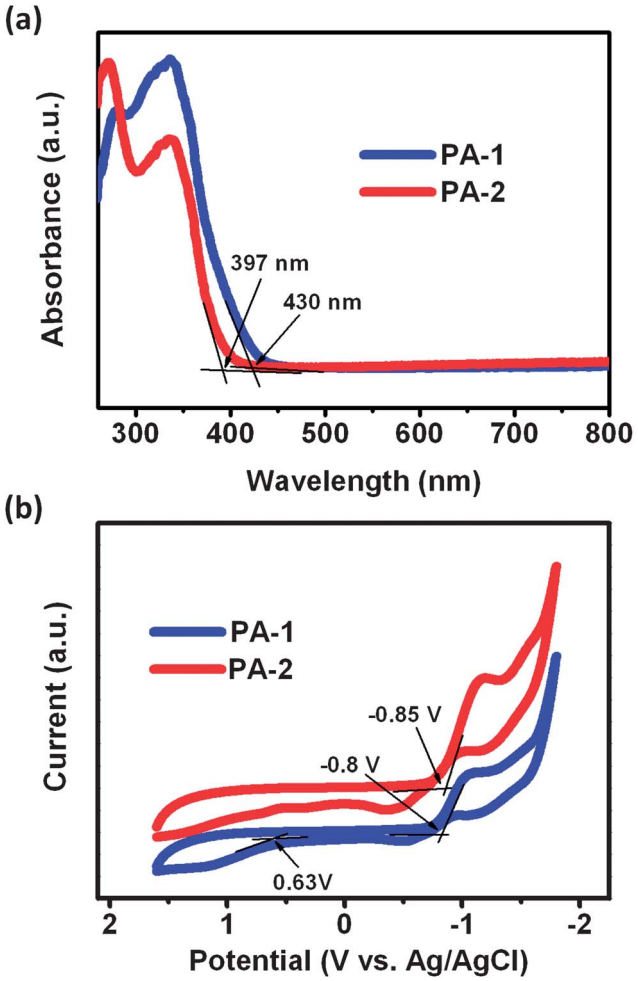

Fig. 1 (a) UV-visible absorption spectra of the free-standing PA films. (b) Cyclic voltammogram profiles of the PA films coated on Pt/Ti/SiO_2/Si substrates.

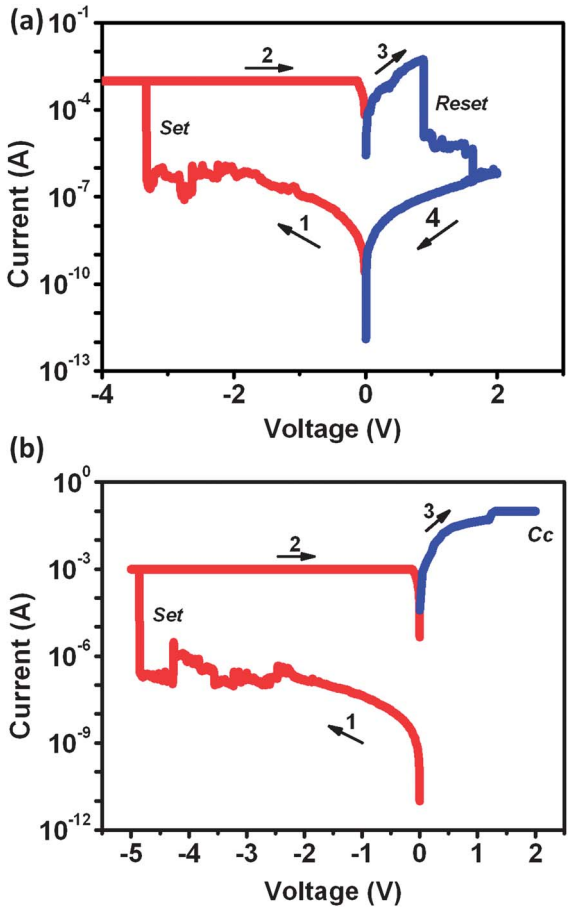

Fig. 2 Current–voltage (*I–V*) characteristics of the (a) Pt/**PA-1**/Pt and (b) Pt/**PA-2**/Pt devices.

Results and discussion

Optical and electrochemical properties

Fig. 1(a) shows the UV-visible absorption spectra of the PA films which were detached from the glass substrate upon casting and dried from the NMP solutions. Both poly(Schiff base)s exhibit two absorption peaks at around 275 nm and 338 nm, respectively, which are attributed to the coupling of the π–π* and n–π* transitions of the imine-containing polymer backbones and the benzene rings of the oxadiazole moieties,[52] and the spin-allowed π–π* transitions involving the azomethine-phenyl-oxadiazole segment.[53] The optical band gaps of **PA-1** and **PA-2**, which are estimated to be 2.88 and 3.12 eV, respectively, are also deduced from the onset optical absorbance wavelength of the polymers.

Fig. 1(b) shows the cyclic voltammogram of the poly(Schiff base) films coated on platinum working electrodes. During the anodic scan, a broad yet moderate oxidation peak of the triphenylamine moieties is observed in the **PA-1** profile with an onset potential of 0.63 V and a peak maximum at 1.17 V, while the oxidation peak in **PA-2** is relatively weak since the oxadiazole unit does not exhibit a strong electron donating ability.

However, the presence of a stronger electron acceptor gives rise to a stronger reduction peak of **PA-2** as compared to that of **PA-1** during the cathodic scan. The reduction peak of **PA-2** is observed with an onset potential of −0.85 V and a peak maximum at −1.16 eV, and the corresponding values for **PA-1** are −0.80 and −1.03 V, respectively. Therefore, the HOMO (highest occupied molecular orbital)/LUMO (lowest unoccupied molecular orbital) energy levels of **PA-1** and **PA-2** are −5.05 eV/−2.17 eV, and −6.70 eV/−3.57 eV, respectively, as deduced according to eqn (S1)–(S4).†

Memory characteristics of the polymers

The resistive switching behaviors of the present poly(Schiff base) films are demonstrated by the current–voltage (*I–V*) characteristics of Fig. 2. At first, platinum was used as the top electrode to fabricate the sandwich devices. As estimated from Fig. 3(a), the initial resistance of the Pt/**PA-1**/Pt device is ~3.2×10^7 Ω, and this state can be defined as the high resistance state (HRS), or off state, of a memory device. As the voltage sweeps from 0 V to −3.3 V, the current of the device increases slowly in the range of 2.0×10^{-10} to 3.4×10^{-7} A. As the sweeping voltage further increases, an abrupt increase of the device current to the magnitude of the compliance current (1 mA) is observed,

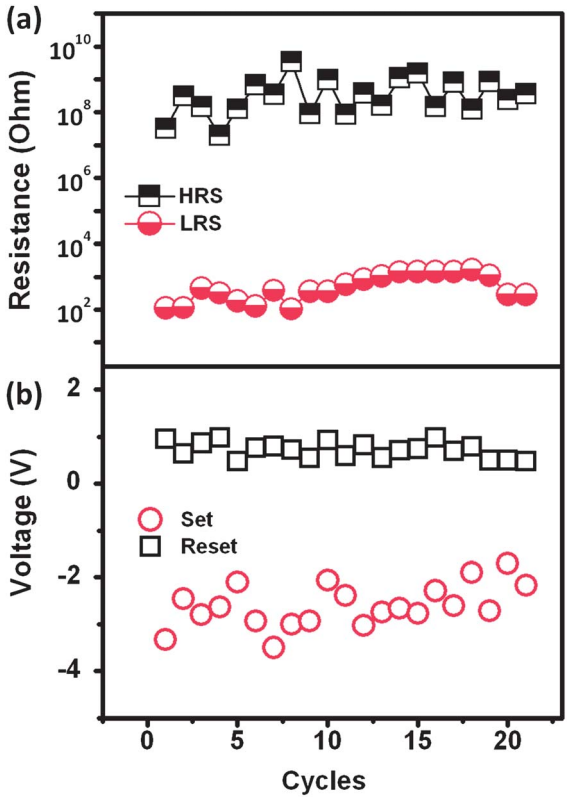

Fig. 3 Endurance performance of the Pt/**PA-1**/Pt device.

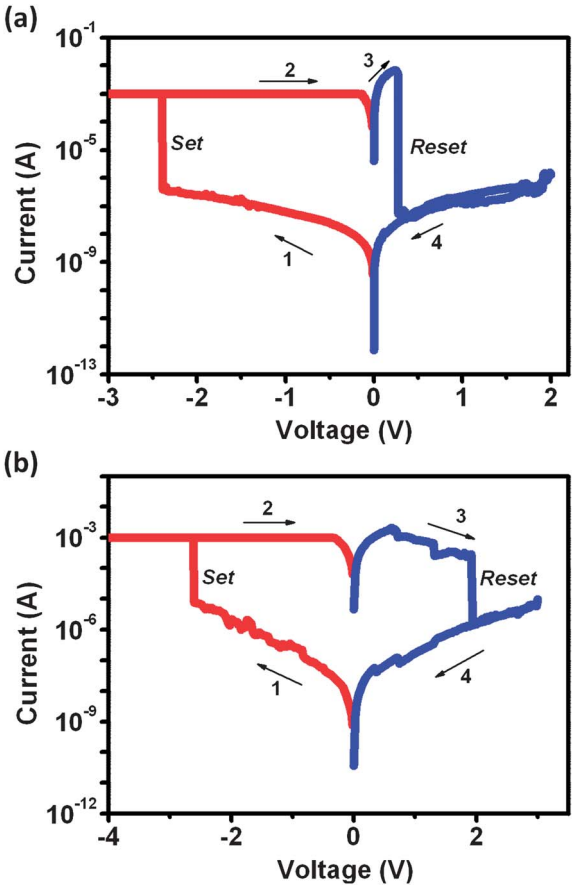

Fig. 4 Current–voltage (*I–V*) curves of the (a) Al/**PA-1**/Pt and (b) Al/**PA-2**/Pt devices.

indicating that the device has been switched from a HRS to a low resistance state (LRS, or on state) (sweep 1 in Fig. 2(a)).

This off-to-on transition can be viewed as the "set" or "write" process in a memory device. The device stays at the on state when the power is turned off or during the following voltage sweep (sweep 2), indicating the non-volatile characteristic of the resistive switching of Pt/**PA-1**/Pt device. A reverse sweeping voltage of 0.9 V can recover the initial off state (sweep 3), and this positively-biased sweeping serves as the "reset" or "erase" process of a rewritable device. It is found that a high on/off ratio (read at 0.1 V) of 10^7 can be achieved in the present device, which leads to a low misreading rate for potential memory applications. However, the transport properties of the Pt/**PA-2**/Pt devices are completely different (Fig. 2(b)). Although the set process is similar to that of the Pt/**PA-1**/Pt device, the threshold voltages (the average switching voltage is −4.6 V for more than 20 tested samples) are found to be larger than that of the Pt/**PA-1**/Pt devices. Moreover, the device could not be reprogrammed to its initial off state with a positive-voltage sweeping operation, and behaves as a typical write-once read-many-times (WORM) memory with an on/off ratio of more than 10^7.

Cyclic switching operations have been conducted to further investigate the endurance performance of the rewritable Pt/**PA-1**/Pt memory devices. Generally, the devices can be repeatedly switched between off and on states for less than thirty cycles. Fig. 3(a) shows the evolution of the resistance of the two well-resolved states for about 20 cycles. The resistance values were read out at 0.1 V in each voltage sweep. The resistance ratios are more than five orders of magnitude during the 20 switching cycles. The resistance of the LRS fluctuates slightly more severely than that of HRS. Fig. 3(b) shows the distribution of the threshold voltages in the cyclic operations. Corresponding to the lighter fluctuation of the LRS resistance, the distribution range of the reset voltages is narrower than that of set process. The average set and reset voltages for the 20 consecutive cycles are −2.6 V and 0.7 V, respectively. The retention performance of Pt/PA/Pt devices, which maintain a stable on/off ratio of more than 10^5 for at least 24 h, is shown in Fig. S3.†

Beyond the chemical structure of the conjugated copolymers that affects the electronic transport properties of the polyazothine derivatives, the choice of electrode metals also plays a key role on the resistive switching behavior of the metal/polymer/metal sandwich structures. With the chemically more active aluminum as top electrodes, the Al/**PA-1**/Pt shows the rewritable resistive switching properties with a set voltage of −2.5 V and a lower on/off ratio of $\sim 10^5$, as shown in Fig. 4(a).

Interestingly, the memory behavior of the **PA-2** based devices changes from that of a WORM type to a rewritable type when the Pt top electrode is replaced by Al (Fig. 4(b)). The on/off ratio for the Al/**PA-2**/Pt is about 3×10^4. Moreover, the current–voltage responses of both the **PA-1** and **PA-2** devices with Al top electrodes are smoother and more stable than those of the

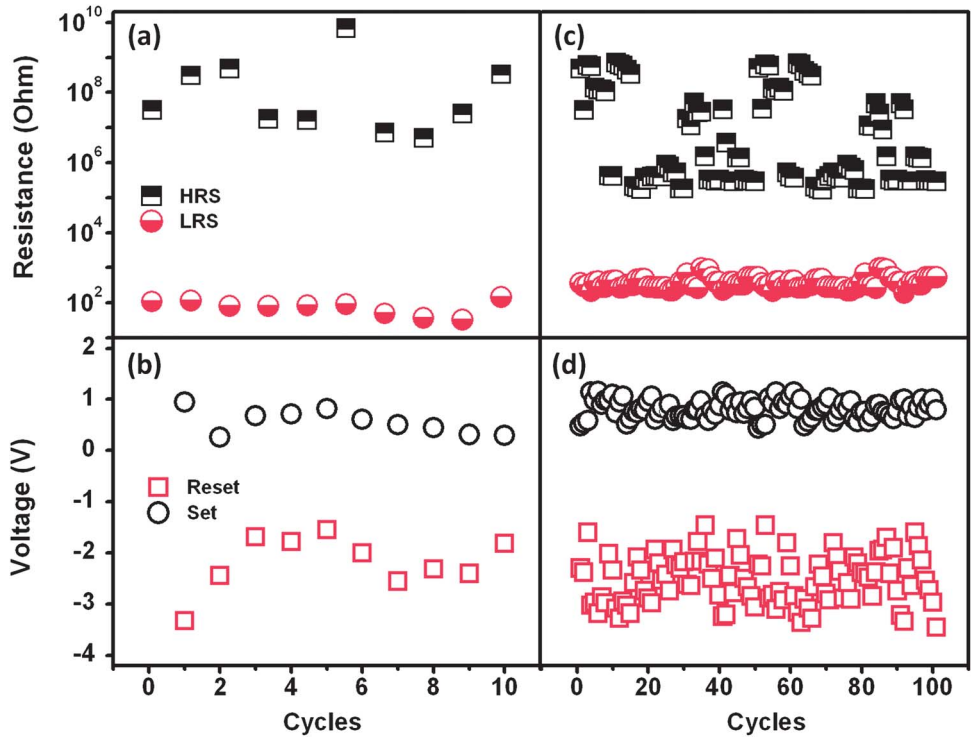

Fig. 5 (a and c) Endurance and (b and d) threshold voltage distribution of the Al/PA/Pt devices.

Pt-electrode devices. The Al/**PA-1**/Pt devices exhibit an on/off operation window of 10^5, and the average set and reset voltages are −2.2 V and 0. 6 V, respectively (Fig. 5(a) and (b)). For the case of the Al/**PA-2**/Pt devices, the on/off window of more than 10^3 can be well maintained for over 100 cycles (Fig. 5(c)). The average set and reset voltages are found to be −2.5 V and 0.8 V, respectively (Fig. 5(d)). Additionally, the retention times of the Al/PA/Pt devices are also longer than 10^5 s, during which no significant degradation of the resistance states was observed (Fig. S4†).

Proposed switching mechanisms

To better understand the switching mechanisms of the metal/PA/metal sandwich structures, molecular simulation, and spectroscopic as well as electrochemical characterization were jointly employed to describe the role of the oxadiazole moiety in the two D–A polyazothines and the electronic scenario of the memory devices. The molecular orbital and electrostatic potential surfaces, calculated and experimental HOMO and LUMO energy levels, and dipole moments of the donor, acceptor and the repeating units of the PAs, together with the

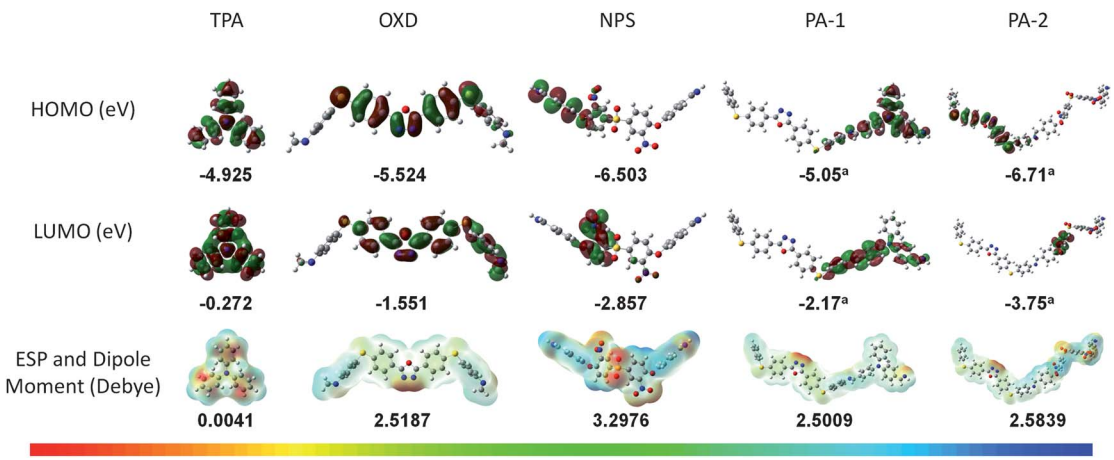

Fig. 6 HOMO, LUMO, electrostatic potential (ESP) surfaces, and dipole moments of TPA, OXD, NPS and PAs. The color bar indicates the revolution of electrostatic potential. [a] Estimated from the UV-visible absorption spectra and CV profiles.

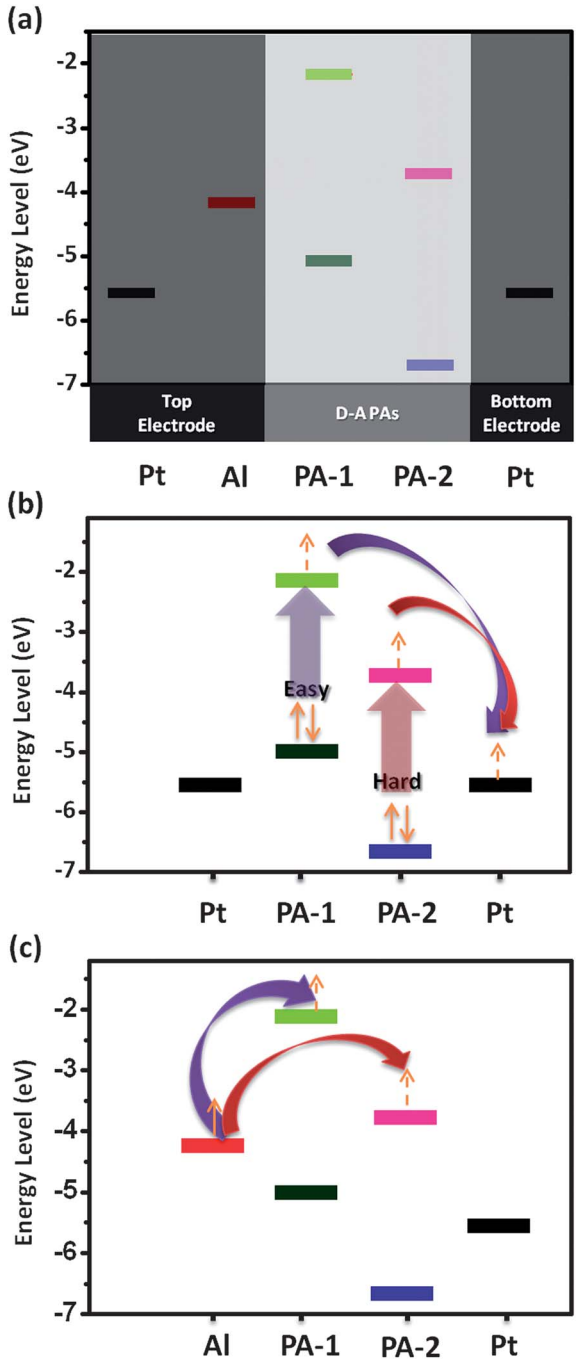

Fig. 7 (a) Energy diagram of M/PA/M sandwich systems, and the different RS mechanisms for the (b) Pt/PA/Pt and (c) Al/PA/Pt devices.

work functions of the metal electrodes, are summarized in Fig. 6 and Fig. 7.

From the molecular orbital energy level diagram of the TPA, OXD and NPS moieties, it can be clearly seen that both the HOMO and LUMO levels of the OXD groups are lower than that of the TPA moieties. Therefore, TPA is the donor component in the **PA-1** D–A structure and OXD is the acceptor component. In comparison with those of the NPS moiety, the molecular orbital energy levels of the OXD group are relatively higher, thus providing the electron donating functionality in the **PA-2** D–A structure. Due to the different roles of the TPA, OXD and NPS groups in the D–A structures of **PA-1** and **PA-2**, it is can be concluded that the HOMO of **PA-1** comes from the TPA donor with its similar energy level, while the LUMO arises from that of the OXD acceptor. Similarly, the HOMO of **PA-2** is from the OXD donor while the LUMO is from the NPS acceptor. In the ground state, the stronger electron donating ability of the TPA moieties leads to more intense charge transfer interactions with the OXD acceptors. Therefore, the pristine **PA-1** thin film demonstrates a lower resistance (read at −1 V) as compared to the pristine **PA-2** thin film. Under a negative electric field with low magnitude, electrons are injected from the electrode into the polymer film and trapped by the OXD acceptors to form a space charge layer, which in turn hinders the further injection of electron charge carriers. At the threshold voltage, charge transfer and separation occur between the TPA and OXD D–A pairs of **PA-1**, as well as between the OXD and NPS moieties of **PA-2**, and the straight arrows in Fig. 7(b) represent the occurrence of electron transition from the HOMO into the LUMO of the polymers. The charge separated state of the D–A pairs increases the carrier concentration inside the solid state polymer thin film significantly, and switches the device from the high resistance state to the low resistance state. The curved arrows in Fig. 7(b) indicate the transport of separated electrons to the metal electrode, which is done in a closed circuit to conduct DC current. Due to the stronger electron push–pull interaction in the D–A structure, the CT effect occurs earlier and more easily in the thin film of **PA-1**, resulting in a lower switching threshold voltage than that of the **PA-2** device. Meanwhile, the moderate electron withdrawing ability of the OXD acceptor makes the CT interaction between the TPA-OXD pairs reversible, and a sufficient reverse electric field can initiate the back transfer of the separated charge carriers. As a result, **PA-1** recovers its initial neutral state and the device returns to its pristine high resistance state with rewritable memory behavior. However, the strong electron withdrawing ability of the NPS moieties causes an irreversible CT interaction between the OXD-NPS pairs, and the **PA-2** based devices behave as a WORM memory. As platinum is chemically inert, the electrode metal in the Pt/PA/Pt devices will not be ionized into cations nor driven into the polymer films under electric fields. The formation of a conductive filament by diffusion of Pt nanoparticles into the polymer thin film during E-beam evaporation process is unlikely to occur either, as the as-fabricated device should be in its initial low resistance state instead of the observed high resistance state. Thus, the resistive switching behaviors in the present Pt-electrode devices may not be accounted for by the formation/rupture of metal filaments.

The dipole moment of the basic unit of the polymers is an important issue that influences the volatility of the resistive switching behaviors, and larger dipole moments favor the retention of separated charge carriers and is beneficial for a non-volatile memory effect. Beyond the dipole moment, there do exist other strategies that will affect the volatility of the polymer memories. For instance, one reported work[54] claimed that by varying the thickness of a thin film constructed from a D–A polymer PI (3,7-APDBT-6FDA) with the small dipole moment of 2.20 debye,

various electrical responses, namely high-conductance ohmic current flow, non-volatile negative differential resistance, dynamic random access memory and insulation are demonstrated. With the azothine-based copolymers carrying larger dipole moments of 2.5009 debye and 2.5839 debye, respectively, which are more favorable for holding separated charge carriers, as well as the much greater thickness (100 nm) of the film which may provide additional trapping centers *via* chain end, chain folds, *etc.*, it is reasonable that the present devices based on **PA-1** and **PA-2** demonstrate non-volatile resistive switching behaviors.

When the Pt electrodes are replaced by the more chemically active metal Al, the Schottky barrier at the metal–polymer interfaces becomes smaller (Fig. 7(c)). Consequently, it is easier for electron injection from Al into the LUMO of **PA-1** to occur (as shown by the curved arrows of Fig. 7(c)), and the Al-electrode devices exhibit lower switching threshold voltages compared to those of the Pt-electrode devices. Similarly, the back transfer also occurs more easily to give a lower reset voltage. It is also noteworthy that the interfacial effect arising from the presence of an ultrathin layer of Al_2O_3 cannot be excluded at the moment, and the resistive switching behaviors of the PAs, **PA-2** in particular, will be affected. For instance, the Al-electrode devices based on **PA-2** demonstrate a rewritable characteristic, rather than the WORM behavior of the Pt-electrode device. To date, the influence of the interfacial effect on the memory behavior of polymer devices is still unclear and is beyond the scope of the present study.

Conclusions

Two D–A type polyazothine derivatives based on triphenylamine, oxadiazole and 3,3′-dinitro-diphenylsulfone moieties have been successfully synthesized for memory device applications. By varying the chemical structure of the electroactive polymers, as well as the top electrode metal, the four kinds of memory devices, Pt/**PA-1**/Pt, Pt/**PA-2**/Pt, Al/**PA-1**/Pt and Al/**PA-2**/Pt, are found to exhibit different resistive switching properties. In the case of the Pt/PA/Pt devices, **PA-1** shows rewriteable memory behavior with poor endurance of less than 20 cycles, while **PA-2** exhibits write-once read-many-times (WORM) memory characteristics. The different memory properties of the Pt-electrode devices originate from the different HOMO–LUMO band gaps of the PAs, which influence the degree of intra- and intermolecular charge transfer interaction between the electron donor–acceptor pairs. By using Al to replace the Pt top electrodes, the Al/PA/Pt devices exhibit a repeatable resistive switching effect, although the endurance of the **PA-1** devices is worse than that of the **PA-2** devices. Besides the reduced Schottky barrier at the metal–polymer interfaces that promotes charge carrier injection from the electrode into the LUMO of the polymer material, the presence of an Al_2O_3 layer may also play an important role in regulating the electrical properties of the metal/polymer/metal sandwich structures.

Acknowledgements

The authors acknowledge financial support from the State Key Project of Fundamental Research of China (973 Program, 2009CB930803, 2012CB933004), the Chinese Academy of Sciences (CAS), the National Natural Science Foundation of China, the Ningbo Science and Technology Innovation Team (2009B21005, 2011B82004), and the Zhejiang and Ningbo Natural Science Foundations.

Notes and references

1 Z. J. Donhauser, B. A. Mantooth, K. F. Kelly, L. A. Bumm, J. D. Monnell, J. J. Stapleton, D. W. Price Jr, A. M. Rawlett, D. L. Allara, J. M. Tour and P. S. Weiss, *Science*, 2001, **292**, 2303.
2 H. Li, Z. Jin, N. Li, Q. Xu, H. Gu, J. M. Lu, X. Xia and L. Wang, *J. Mater. Chem.*, 2011, **21**, 5860.
3 B. Cho, S. Song, Y. Ji, T. W. Kim and T. J. Lee, *Adv. Funct. Mater.*, 2011, **21**, 2806–2829.
4 N. G. Kang, B. Cho, B. G. Kang, S. Song, T. J. Lee and J. S. Lee, *Adv. Mater.*, 2012, **24**, 385–390.
5 S. M. Miao, Y. X. Zhu, H. Zhuang, X. P. Xu, H. Li, R. Sun, N. J. Li, S. J. Ji and J. M. Lu, *J. Mater. Chem. C*, 2013, **1**, 2320.
6 Y. G. Ko, W. Kwon, H. J. Yen, C. W. Chang, D. M. Kim, K. Kim, S. G. Hahm, T. J. Lee, G. S. Liou and M. Ree, *Macromolecules*, 2012, **45**, 3749.
7 S. J. Liu, W. P. Lin, M. D. Yi, W. J. Xu, C. Tang, Q. Zhao, S. H. Ye, X. M. Liu and W. Huang, *J. Mater. Chem.*, 2012, **22**, 22964.
8 C. J. Chen, Y. C. Hu and G. S. Liou, *Chem. Commun.*, 2013, **49**, 2536.
9 H. Li, Q. Xu, N. Li, R. Sun, J. Ge, J. M. Lu, H. Gu and F. Yan, *J. Am. Chem. Soc.*, 2010, **132**, 5542.
10 X. D. Zhuang, Y. Chen, G. Liu, P. P. Li, C. X. Zhu, E. T. Kang, K. G. Noeh, B. Zhang, J. H. Zhu and Y. X. Li, *Adv. Mater.*, 2010, **22**, 1731.
11 Y. Ma, X. Cao, G. Li, Y. Wen, Y. Yang, J. Wang, S. X. Du, L. M. Yang, H. Gao and Y. L. Song, *Adv. Funct. Mater.*, 2010, **20**, 803.
12 F. Zhao, J. Liu, X. Huang, X. Zou, G. Lu, P. Sun, S. Wu, W. Ai, M. Yi, X. Qi, L. Xie, J. Wang, H. Zhang and W. Huang, *ACS Nano*, 2012, **6**, 3027.
13 K. Kim, H. J. Yen, Y. G. Ko, C. W. Chang, W. Kwon, G. S. Liou and M. Ree, *Polymer*, 2012, **53**, 4135.
14 G. Liu, Q.-D. Ling, E.-T. Kang, K.-G. Neoh, D. J. Liaw, F. C. Chang, C.-X. Zhu and D. S. H. Chan, *J. Appl. Phys.*, 2007, **102**, 024502.
15 B. Hu, R. Quhe, C. Chen, F. Zhuge, X. Zhu, S. Peng, X. Chen, L. Pan, Y. Wu, W. Zheng, Q. Yan, J. Lu and R.-W. Li, *J. Mater. Chem.*, 2012, **22**, 16422.
16 B. Y. Ji, B. Cho, S. Song, T. W. Kim, M. Choe, Y. H. Kahng and T. Lee, *Adv. Mater.*, 2010, **22**, 3071.
17 G. Liu, B. Zhang, Y. Chen, C.-X. Zhu, L. Zeng, D. Siu-Hung Chan, K.-G. Neoh, J. Chen and E.-T. Kang, *J. Mater. Chem.*, 2011, **21**, 6027.
18 B. Hu, X. Zhu, X. Chen, L. Pan, S. Peng, Y. Wu, J. Shang, G. Liu, Q. Yan and R.-W. Li, *J. Am. Chem. Soc.*, 2012, **134**, 17408.
19 J. J. Yang, M. D. Pickett, X. Li, D. A. A. Ohlberg, D. R. Stewart and R. S. Williams, *Nat. Nanotechnol.*, 2008, **3**, 429.

20 A. Iwan and D. Sek, *Prog. Polym. Sci.*, 2008, **33**, 289.
21 A. Nayak, T. Ohno, T. Tsuruoka, K. Terabe, T. Hasegawa, J. K. Gimzewski and M. Aono, *Adv. Funct. Mater.*, 2012, **22**, 3606.
22 S. Yu, B. Gao, Z. Fang, H. Yu, J. Kang and H. S. P. Wong, *Adv. Mater.*, 2013, **25**, 1774.
23 S. H. Jo, T. Chang, I. Ebong, B. B. Bhadviya, P. Mazumder and W. Lu, *Nano Lett.*, 2010, **10**, 1297.
24 M. Ziegler, R. Soni, T. Patelczyk, M. Ignatov, T. Bartsch, P. Meuffels and H. Kohlstedt, *Adv. Funct. Mater.*, 2012, **22**, 2744.
25 W. Lu, *Nat. Mater.*, 2013, **12**, 93.
26 M. D. Pickett, G. Medeiros-Ribeiro and R. S. Williams, *Nat. Mater.*, 2013, **12**, 114.
27 Q. Xia, W. Robinett, M. W. Cumbie, N. Banerjee, T. J. Cardinali, J. J. Yang, W. Wu, X. Li, W. M. Tong, D. B. Strukov, G. S. Snider, G. Medeiros-Ribeiro and R. S. Williams, *Nano Lett.*, 2009, **9**, 3640.
28 J. Borghetti, G. S. Snider, P. J. Kuekes, J. J. Yang, D. R. Stewart and R. S. Williams, *Nature*, 2010, **464**, 873.
29 Q. D. Ling, F. C. Chang, Y. Song, C. X. Zhu, D. J. Liaw, D. S. H. Chan, E. T. Kang and K. G. Neoh, *J. Am. Chem. Soc.*, 2006, **128**, 8732.
30 E. E. Havinga, W. Tenhoeve and H. Wynberg, *Polym. Bull.*, 1992, **29**, 119.
31 V. Mullekom, J. Vekemans, E. E. Havinga and E. W. Meijer, *Mater. Sci. Eng., R*, 2001, **32**, 1.
32 P. M. Beaujuge, C. M. Amb and J. R. Reynolds, *Acc. Chem. Res.*, 2010, **43**, 1396.
33 S. G. Hahm, S. Choi, S. H. Hong, T. J. Lee, S. Park, D. M. Kim, W. S. Kwon, K. Kim, O. Kim and M. Ree, *Adv. Funct. Mater.*, 2008, **18**, 3276.
34 J. Hu, Y. Li, Z. Ji, G. Jiang, L. Yang, W. Hu, H. Gao, L. Jiang, Y. Wen, Y. L. Song and D. Zhu, *J. Mater. Chem.*, 2007, **17**, 3530.
35 Q. Liu, K. Jiang, L. Wang, Y. Wen, J. Wang, Y. Ma and Y. Song, *Appl. Phys. Lett.*, 2010, **96**, 213305.
36 J. J. Yang, D. B. Strukov and D. R. Stewart, *Nat. Nanotechnol.*, 2013, **8**, 13.
37 T. Kurosawa, Y. C. Lai, T. Higashihara, M. Ueda, C. L. Liu and W. C. Chen, *Macromolecules*, 2012, **45**, 4556.
38 T. Kurosawa, Y. C. Lai, A. D. Yu, H. C. Wu, T. Higashihara, M. Ueda and W. C. Chen, *J. Polym. Sci., Part A: Polym. Chem.*, 2013, **51**, 1348.
39 J. C. Chen, Y. C. Liu, J. J. Ju, C. J. Chiang and Y. T. Chern, *Polymer*, 2011, **52**, 954.
40 A. Bolduc, S. Dufresne and W. G. Skene, *J. Mater. Chem.*, 2010, **20**, 4820.
41 S. Barik and W. G. Skene, *Macromolecules*, 2010, **43**, 10435.
42 H. H. Chang, C. E. Tsai, Y. Y. Lai, D. Y. Chiou, S. L. Hsu, C. S. Hsu and Y. J. Cheng, *Macromolecules*, 2012, **45**, 9282.
43 G. Hughes and M. R. Bryce, *J. Mater. Chem.*, 2005, **15**, 94.
44 J. A. Mikroyannidis, I. K. Spiliopoulos, T. S. Kasimis, A. P. Kulkarni and S. A. Jenekhe, *Macromolecules*, 2003, **36**, 9295.
45 Y. L. Liu, K. L. Wang, G. S. Huang, C. X. Zhu, E. S. Tok, K. G. Neoh and E. T. Kang, *Chem. Mater.*, 2009, **21**, 3391.
46 Y. K. Fang, C. L. Liu and W. C. Chen, *J. Mater. Chem.*, 2011, **21**, 4778.
47 W. Kwon, B. Ahn, D. M. Kim, Y. G. Ko, S. G. Hahm, Y. Kim, H. Kim and M. Ree, *J. Phys. Chem. C*, 2011, **115**, 19355.
48 L. Zeng, G. Liu, B. Zhang, J. Chen, Y. Chen and E. T. Kang, *Polym. J.*, 2012, **44**, 257.
49 Y. Imai, M. Ueda and K. Otaira, *J. Polym. Sci., Polym. Chem. Ed.*, 1977, **15**, 1457.
50 D. Sek, A. Iwan, B. Jarzabek, B. Kaczmarczyk, J. Kasperczyk, Z. Mazurak, M. Domanski, K. Karon and M. Lapkowski, *Macromolecules*, 2008, **41**, 6653.
51 M. J. Frish, G. W. Trucks, H. B. Schiegel, G. E. Scuseria, M. A. Robb and J. R. Cheeseman, *Gaussian 09 (Revision A.02)*, Gaussian Inc., Wallingford CT, 2009.
52 E. Wolarz, E. Chrzumnicka, T. Fischer and J. Stumpe, *Dyes Pigm.*, 2007, **75**, 753.
53 L. Marin, M. D. Damaceanu and D. Timpu, *Soft Mater.*, 2009, **7**, 1.
54 C. L. Liu, T. Kurosawa, A. D. Yu, T. Higashihara, M. Ueda and W. C. Chen, *J. Phys. Chem. C*, 2011, **115**, 5930.

